[1]College of Science & Engineering, Flinders University, Adelaide, Australia

Corresponding author: Jochen Kämpf (jochen.kaempf@flinders.edu.au)

Key Points:

- Wind-driven surface currents induce nutrient upwelling around atoll reefs that fuel subsurface phytoplankton blooms
- Both enhanced rainfall extremes and sea level rise can significantly reduce phytoplankton production around atolls
- These climate-change effects will cause disruptions to the functioning of marine ecosystems in tropical oceans

Abstract

Using the method of process-oriented hydrodynamic modelling, this study explores wind-driven upwelling features around atoll reefs. The three-dimensional physical model is coupled to a biological model to simulate phytoplankton blooms initiated by the upwelling. Findings demonstrate that wind forcing can create a zone of nutrient upwelling near atolls reefs fueling significant subsurface phytoplankton blooms. Here we show that both lowering surface salinity due to enhanced precipitation, and submergence of the atoll reef due to sea level rise and enhanced erosion lead to a significant reduction of phytoplankton productivity. We expect that this climate-change related reduction in phytoplankton production around atoll reefs will cause severe disruptions to the functioning of marine ecosystems in tropical oceans.

Plain Language Summary

Atoll reefs provide the habitat for productive marine ecosystems that serve as feeding stations for a rich variety of local and migrating marine species. Phytoplankton blooms are often the foundation of localized marine food chains. Here we show that significant subsurface phytoplankton blooms can form near atoll reefs under the action of surface winds. In conjunction with global sea level rise, climate models predict an increase in rainfall in tropical regions, where many atoll reefs are situated. Here we show that these features have the potential to significantly reduce phytoplankton production around atoll reefs, causing severe disruptions to the functioning of marine ecosystems in tropical oceans.

1 Introduction

Atolls are ring-shaped reefs that occur in the open ocean, often arranged in archipelagoes or linear island chains. Most atolls are located in the Pacific Ocean, but there are also numerous atolls in the central Indian Ocean. The platforms of atolls are generally characterized by reefs that reach sea level. Atoll widths vary between a few hundred to dozens of kilometers. There is considerable variation in the geometry of reef crests around the perimeter of the central lagoon, ranging from continuous to highlight fractured. Overall, there exist 1,770 ocean islands, including 47 active volcanoes and ~440 atolls (see Watts,

2019). Satellite-derived gravity and ship data show there are >14,500 seamounts higher than 1 km, including numerous submerged shoals, that unlike atolls do not reach the sea level. Atolls display a wide variety of shapes (e.g. Stoddart, 1965) and occur across a wide range of climatic and oceanographic conditions (e.g. Bryan, 1953). Charles Darwin (1842) produced the first global map of the distribution of known atolls and other reef types.

A key difference between atoll reefs and continental margins is the absence of a shelf. Instead, the outer reef of atolls is characterized by steep reef fronts with slopes of up to 45°. Reef fronts often have one or more distinct terraces, a few tens of meters wide. Shallow reef fronts are dominated by "spur-and-groove" morphology (Munk and Sargent, 1954) that consist of ridges (spurs) and channels (grooves) running at right angles to the reef margin in depths of up to 30 m. Typical spur heights are 0.5-10 m, and grooves are 1-100 m wide (Rogers, 2015). Submarine channels (gullies), a few kilometers wide, are embedded in the flanks for larger atolls, such as the Ontong Java and Nukumanu atolls (western equatorial Pacific Ocean) (Watson et al., 2017). Such channels are deemed important for the exchange of seawater in and out of the lagoon and as downslope conduits for turbidity currents that transport suspended sediment into depths through connected deep-sea canyons.

Groups of islands are often associated with enhanced plankton productivity due to various physical mechanisms, often summarized as "island mass effect" (Doty and Oguri, 1956) or ''island stirring'' (Mann and Lazier, 1991). This effect has been attributed to strong tidal flows enhancing vertical mixing and breaking down the nutricline, tidally induced internal waves pumping nutrient-rich subsurface water onto the reef (Griffin et al., 1987), and the formation of island wakes, lee eddies and upwelling features induced by the topographic effects on ambient geostrophic currents (Messié et al., 2020). Localized wind–front interactions can create upwelling of nutrients at the Galápagos Islands (Forryan et al., 2021), which is located near the equator in the eastern Pacific. Away from the equator, wind-stress forcing creates surface Ekman layers that create coastal upwelling on one side of an island and downwelling on the other side (Spall and Pedlosky, 2013). In how much wind-driven upwelling induces nutrient enrichment near exposed or submerged atoll reefs is unknown.

There is indirect evidence of enhanced biological productivity near atoll reefs. For instance, a preliminary study on the fisheries catches in South China Sea using light falling nets (Wu et al., 2016) documented significant squid and tuna stocks around both the Paracel Islands and the Spratly Islands, which are regions of numerous atolls and shoals. With a net spanning an area of 3150 m^2 (equivalent to 63m by 50m), the average fishing rate was ~470 kg/h with purpleback flying squid (*Stenouteuthis oualaniensis*) comprising ~60% and yellowfin tuna (*Thunnus albacares*), skipjack tuna (Katsuwonus pelamis), and mackerel scads (Decapterus maruadsi) together comprising ~40% of the total catch. The "island mass effect" around the Paracel Islands and the Spratly Islands may explain why the South China Sea supports annual fish catches of the same order

of magnitude as the world's most productive upwelling system off the coasts of Peru and Chile (Kämpf and Chapman, 2016).

The island mass effect can be inferred from satellite derived chlorophyll-a level as a proxy for surface phytoplankton concentrations. These surface signals are generally 1-2 order of magnitude smaller (0.1-0.5 mg/m^3 in chl-*a*) than those characterizing major upwelling systems (5-10 mg/m^3 in chl-*a*). For example, ship data around Madeira Island, Northeast Atlantic. indicate maximum surface chl-*a* values of 0.15 mg/m^3 (Caldeira et al., 2002). Values of up to 0.7 mg/m^3 in surface chl-*a* were observed using satellite data over distances of several hundred kilometers from the Tonga Islands, Southwest Pacific (Messié et al., 2020).

In contrast, surface chl-*a* levels in the open ocean and near atolls are generally very low (<0.1 mg/m3) and are often not detectable from space. However, phytoplankton biomass often increases deeper in the water column, reaching a subsurface maximum that can be far greater than that observed in surface waters. For instance, Furuya (1990) detected enhanced chl-*a* levels of 0.3-0.4 mg/m^3 at a depth of ~100 m in the western Pacific. Findings by Gove et al. (2016) showed a significant increase of depth-integrated chl-*a* levels (dominated by subsurface signals) within 10 km from the coast from 25 in situ surveys across 21 Pacific coral reef islands and atolls with values in a range of 1-10 mg/m^2.

Many atoll reefs are located in regions where significantly more heavy rainfall extremes are to be expected due to global climate change by the end of this century (Fischer et al., 2014). The resultant reductions in surface salinity and density in surface layers of the ocean, characteristic of so-called barrier layers (see Sprintall and Tomczak, 1992), may influence the biologic productivity around atoll reefs. On longer timescales (>100 years) the global sea level may rise by several meters, which will lead to the submergence of many atoll reefs, further enhanced due to wave erosion (e.g. Bramante et al., 2020). Using the method of process-oriented hydrodynamic modelling, this work explores the formation of phytoplankton blooms around atoll reefs and its response to changes in surface salinity and changes in the sea level.

2 Methodology

2.1 Model description

This study applies the hydrodynamic model COHERENS (Luyten et al., 1999). The governing equations are the finite-difference forms of conservation equations for momentum, heat, volume and scalars for an incompressible fluid on the *f* plane cast in terrain-following sigma coordinates. COHERENS is based on the same physical laws and coordinate transformation and similar numerical algorithms that govern other sigma coordinate models such as POM (Blumberg and Mellor, 1987) or ROMS (Shchepetkin and McWilliams, 2005). For simplicity, the Coriolis parameter is set to f = $+1\times10^{-4}$ s^{-1}. Horizontal turbulence is parameterized using the closure scheme by Smagorinsky (1963). Vertical turbulence is parameterized using a simple level 2.5 closure of Mellor and Yamada (1982) with the modifications introduced by Galperin et al. (1988). Bottom friction is

parameterized using a quadratic approach based on a bed roughness length of 2 mm. Variations of turbulence parameters had no significant influence on the results. A linear equation of state is used to calculate density anomalies from anomalies of temperature and salinity, each predicted by an advection-diffusion equation. The same equation is used to predict anomalies of a conservative nutrient tracer, taken as a proxy of dissolved nitrogen concentration.

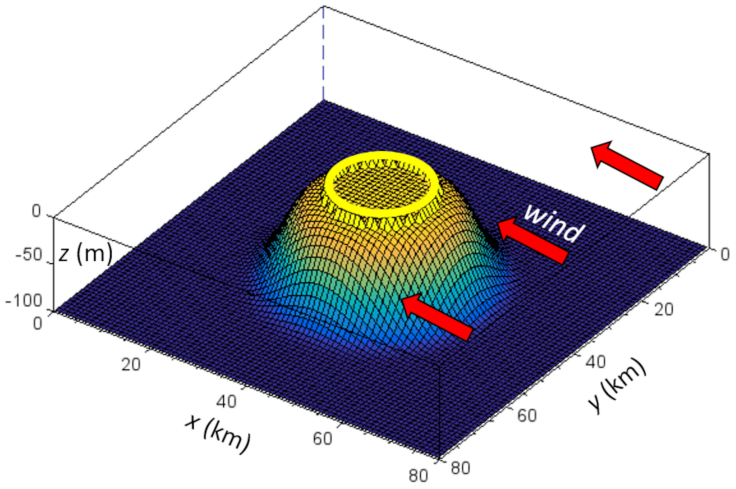

Figure 1: Model domain and configuration of a simplified atoll reef considered in this study.

The biological response to changes in the nutrient distribution is derived from application of a NPZD (Nitrogen-Phytoplankton-Zooplankton-Detritus) model, described in detail by Ji et al. (2008). This study focuses on the initial phytoplankton response on timescales of 5-10 days. For simplicity, effects due to zooplankton and detritus are neglected. We applied the same parameter settings as Ji et al. (2008). Using the nutrient distribution predicted by the hydrodynamic model as initial condition, the NPZD model is forced by a surface radiance varying as function of the day-night cycle according to:

$$I_o(t) = max\left[I_{oo} sin(\tfrac{2\pi t}{T}, 0\right] \quad (1)$$

where I_{oo} is set to 800 Wm^{-2}, t is time and T is the duration of a day. Initial phytoplankton concentrations are uniform with a small values of 0.1 M-N. Chlorophyll-a levels are calculated from an average C:chl-a ratio of 50:1 (see Jakobsen and Markager, 2016) and a Redfield ratio of C:N of 106:16. This yields a conversion ratio between phytoplankton in units of M-N and chlorophyll-a in units of mg C/m^3 of 1:1.855.

2.2 Experimental design

The model bathymetry is a simplified circular reef, 20 km in diameter, consisting of lagoon, 10 m deep, and a ring-shaped reef top (**Figure 1**). Additional

bathymetric features such as channel fractures are ignored here. In a series of experiments, the reef top either forms an island, or it is submerged to depths of up to 8 m. The depth of the lagoon, kept at 10 m, does not influence the results. The reef is cast in a model domain of 80 km by 80 km in horizontal dimension, resolved by a horizontal grid spacing of 500 m. The vertical extent of the domain is limited to 100 m, resolved by 10 sigma layers, noting that strong density stratification applied to the upper ocean hinders the creation of significant currents below the pycnocline. Zero-gradient conditions are used at all horizontal boundaries. Sea-level anomalies are kept at zero values along the southern boundary.

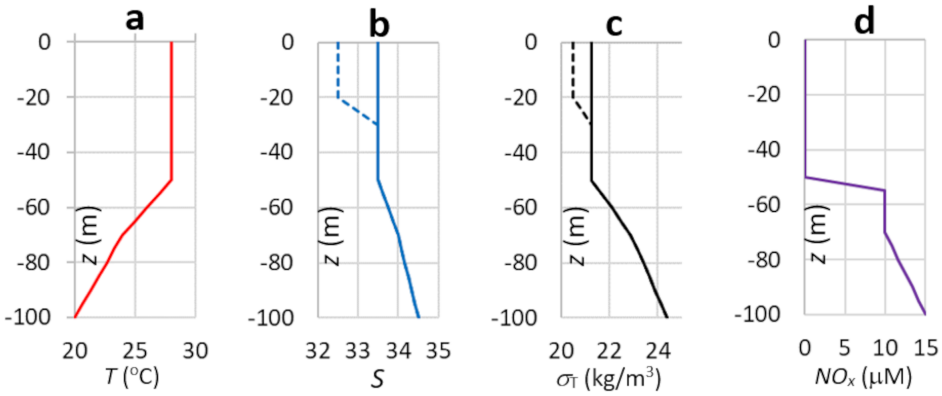

Figure 2: Model configuration. Initial vertical profiles of a) temperature (°C), b) salinity, c) density excess above 1000 kg/m^3 ($_T$; kg/m^3), and d) nitrogen as dissolved nitrate concentration (M). Dashed lines show the addition of a low-salinity surface layer that creates a barrier layer in the depth range of 20 to 50 m.

Vertical temperature and salinity stratifications mimic the typical tropical situation with a warm and low-salinity surface mixed layer followed by colder and more saline water underneath (**Figure 2**). The thermocline is located at a depth of 50 m (Fig. 2a). In a series of experiments, a barrier layer is added via lowering the salinity of the upper 20 m of the water column by up to 1 salinity units (Fig. 2b), which creates a strong pycnocline at a depth range of 20-25m (Fig. 2c). The barrier layer is a typical feature of the tropics (e.g. Sprintal and Tomczak, 1992). Changes in surface salinity, considered here, mimic the future increase in rainfall extremes. Initially, the uppermost 50 m of the water column is depleted in nitrogen (Fig. 2d). In the depth range of 50-70 m, the nitrate concentration is set to 10 M, increasing linearly to 15 M at a depth of 100 m.

The model is forced by a uniform westward wind of a wind stress of 0.15 Pa, corresponding to a wind speed of 10 m/s. The wind field is blended in over the first simulation day to avoid initial dynamical disturbances. The total simulation time of hydrodynamic model runs is 5 days. The final model outputs are then used as initial conditions for the NPZD model, interpolated to an equidistant

vertical grid spacing of 1 m. The NPZD model is then run for another 10 days to simulate the phytoplankton response to the wind-induced anomalies in the nutrient field.

The results of a total of 25 simulations are discussed here. This includes all combinations of salinity reductions in the upper 20 m of the water column of S = 0, 0.25, 0.5, 0.75 and 1, and lowering the depth of the atoll ring from H = 0 m (ie. an island) to depths of 2 m, 4m, 6m and 8 m.

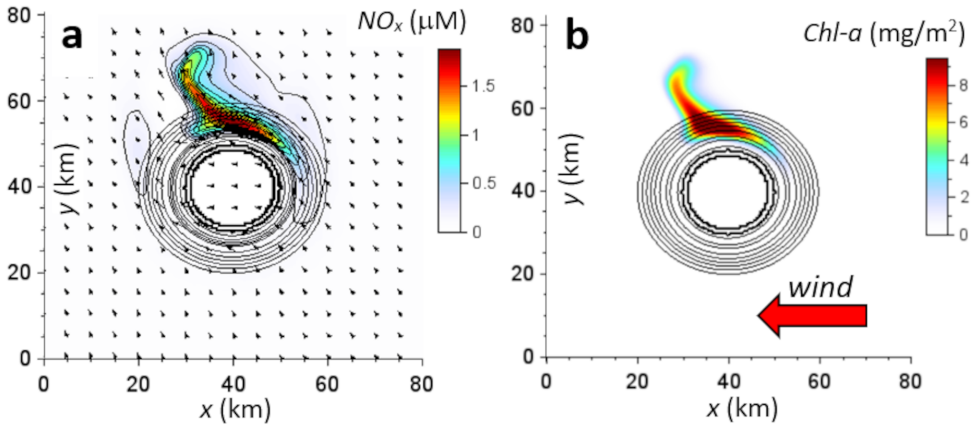

Figure 3: a) Surface distribution of dissolved nitrogen concentrations (µM) after 5 days of simulation of the hydrodynamic model. b) Horizontal distribution of vertically integrated chlorophyll-a concentrations (mg/m^2) after 10 days of simulations with the NPZD model.

4 Results and Discussion

Let us first consider the phytoplankton production around a closed atoll that forms an island in the oceanographic sense ($H = 0$) and the absence of a barrier layer ($S = 0$). The wind forcing creates a surface Ekman layer with a classical Ekman spiral extending to 20-30 m depth. The Ekman currents interact with the reef to create zones of horizontal divergence, inducing upwelling on one side of the reef, and divergence, inducing downwelling on the other side of the reef, as described by Spall and Pedlosky (2013) for islands. The upwelling process creates a zone of elevated nutrient concentration in the upwelling center on the northern side of the atoll (Figure 3a). Here, the wind forcing also creates a coastal upwelling jet that injects the nutrient-enriched water as a filament into the ambient ocean.

The distribution of vertically integrated biomass (Figure 3b) matches the nutrient distribution (see Fig. 3a). The highest values of 10 mg/m^2 are found in the upwelling center close to the atoll. The magnitude of values agrees with observational evidence (Gove et al., 2016). Note that the maximum phytoplankton growth occurs below the surface at a depth of 20 m, where chlorophyll-a levels of ~1 mg/m^3 form (Figure 4). Surface chlorophyll-a values are <0.5 mg/m^3.

Overall, the upwelling leads to the creation of 263.5 kg/day of chlorophyll-a.

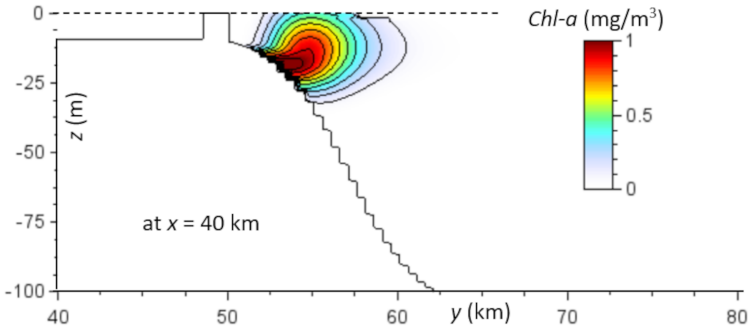

Figure 4: Vertical transect at $x = 40$ km of chlorophyll-a concentrations (mg/m^3) after 10 days of simulations with the NPZD model.

A couple of points are worth noting here. Firstly, this upwelling around atoll reefs occurs independent of the wind direction, which is fundamentally different from the classical coastal upwelling mechanism that can be characterized by an upwelling index (Kämpf and Chapman, 2016). Secondly, this upwelling and phytoplankton production around atoll reefs can be a continuous process lasting several months in regions exposed to monsoon winds.

Let us now see in how much surface salinity and submergence level of the reef influence the overall phytoplankton productivity (Table 1). Physically, the addition of a layer of low salinity surface water enhances static stability of the water column which lowers upward turbulent nutrient fluxes. Enhanced static stability also slows down and weakens the upwelling signal (Kämpf and Kavi, 2019). For the case $H = 0$, the rate of chlorophyll-a production decreases by 57% for $S = 0.25$ compared with the reference case of $S = 0$, 85% for $S = 0.5$, 98% for $S = 0.75$, and 99% for $S = 1$. When selecting a reference case of $S = 0.25$ (corresponding to a chl-a production rate of 114 kg/day), then this rate decreases by 65% for $S = 0.5$, 95% for $S = 0.75$, and 98% for $S = 1$. Hence, enhanced rainfall extremes have the potential to substantially decrease phytoplankton productivity around atoll islands.

Submergence of the atoll reef influences the upwelling process in a different way. The submergence level, H, influence the depth level below which Ekman currents induce horizontal divergence/convergence with the reef structure. In the classical Ekman spiral, the horizontal current speed decreases exponentially with depth. Hence, wind-driven Ekman layers can only "feel" atoll reefs that are located close to the sea surface, and the upwelling intensity decreases for higher submergence levels. With $S = 0$ and relative to $H = 0$, for instance, the chlorophyll-a production rate decreases by 29% for $H = 2$ m, 62% for $H = 4$ m, 78% for $H = 6$ m and 84% for $H = 10$ m. With $S = 2.5$ and relative to $H = 0$, for instance, the chlorophyll-a production rate decreases by 51% for $H = 2$ m, 89% for $H = 4$ m, 98% for $H = 6$ m and 99% for $H = 10$ m.

The effects due to increases in S and H are additive. Let us reconsider the reference case of $S = 0.25$ and relative to $H = 0$. An increase to $S = 0.5$ decreases the chl-a production rate by 65%, whereas and increase to $H = 2$ m decreases it by 51%. However, a combined change of both S and H decreases the chl-a production rate by 91%.

Table 1: Total rate of chlorophyll-a production (kg/day) predicted by the NPZD model

ΔH (m) \ ΔS	0	0.25	0.5	0.75	1
0	263.53	114.04	40.25	5.07	2.22
2	187.09	56.40	10.36	2.98	2.34
4	99.83	12.91	1.69	0.89	0.85
6	56.80	2.09	0.27	0.17	0.22
8	41.16	0.63	0.06	0.04	0.06

5 Conclusions

Studies on climate-change impacts on the world's largest upwelling systems have received considerable attention in the past decades (e.g., Abrahams, 2020). Here we show that winds forcing can create substantial subsurface phytoplankton blooms over atoll reefs in a quasi-continuous manner. This is a significant finding given the large number of atoll reefs and islands that exist in the oceans. The combined effect of increasing submergence levels of atoll reefs due to global sea level rise and erosion and enhanced surface salinities due to more rainfall extremes has the potential to shutdown phytoplankton production around atolls and associated marine food webs in most of the tropical Pacific and Indian Ocean.

Acknowledgments

The author has no real or perceived financial conflicts of interests of any part of this research. This work did not receive external funding, but it was supported by an internal research grant from the Marine and Coastal Science Consortium, Flinders University.

Data Availability Statement

This work did not use new data.

Open Research

The latest version of the COHERENS model can be downloaded at: https://odnature.naturalsciences.be/coherens/. A user manual is available at: https://uol.de/f/5/inst/icbm/ag/physoz/download/from_emil/COHERENS/print/userguide.pdf (accessed on 15.12.21).

References

Abrahams A., Schlegel R. W., & Smit A. J. (2021), Variation and change of upwelling dynamics detected in the world's eastern boundary upwelling systems. *Frontiers in Marine Science, 8.* doi:10.3389/fmars.2021.626411

Blumberg, A. F., & Mellor, G. L. (1987), A description of a three-dimensional coastal ocean circulation model. In: Heaps, N.S. (Ed.), Three-Dimensional Coastal Ocean Models. Book 4, American Geophysical Union, 1-6. doi:10.1029/CO004p0001

Bramante, J. F., Ashton, A. D., Storlazzi, C. D., Cheriton, O., & Donnelly, J.P. (2020), Sea-level rise will drive divergent sediment transport patterns on fore reefs and reef flats, potentially causing erosion on atoll islands. *Journal of Geophysical Research – Earth Surface, 125(11).* doi: 10.1029/2019JF005446

Bryan, E. H., Jr. (1953), Check list of atolls. *Atoll Research Bulletin, 19,* 1–38. doi:10.5479/si.00775630.19.1

Caldeira, R.M.A., Groom, S., Miller, P., Pilgrim, D., & Nezlin, N.P. (2002), Sea-surface signatures of the island mass effect phenomena around Madeira Island, Northeast Atlantic. *Remote Sensing of Environment, 80(2)*, 336–360. doi:10.1016/S0034-4257(01)00316-9

Darwin, C. (1842), Structure and distribution of coral reefs, South Elder and Co., London, 207 pp. Available online: http://darwin-online.org.uk/converted/published/1842_Coral_F271/1842_

Doty, M. S., & Oguri, M. (1956), The island mass effect. *Journal du Conseil Permanent International pour l'Exploration de la Mer, 22*, 33–37.

Fischer, E. M., Sedláček, J., Hawkins, E., & Knutti, R. (2014), Models agree on forced response pattern of precipitation and temperature extremes, *Geophysical Research Letters, 41*, 8554–8562. doi:10.1002/2014GL062018

Forryan, A., Naveira Garabato, A. C., Vic, C., et al. (2021) Galápagos upwelling driven by localized wind–front interactions. *Scientific Reports, 11,* 1277. doi:10.1038/s41598-020-80609-2

Furuya, K. (1990), Subsurface chlorophyll maximum in the tropical and subtropical western Pacific Ocean: Vertical profiles of phytoplankton biomass and its relationship with chlorophyll-a and particulate organic carbon. *Marine Biology, 107*, 529–539.

Galperin, B., Kantha, L. H., Hassid, S., & Rosati, A., (1988), A quasi-equilibrium turbulent energy model for geophysical flows. *Journal of the Atmospheric Sciences, 45,* 55–62.

Gove, J., McManus, M., Neuheimer, A., et al. (2016), Near-island biological hotspots in barren ocean basins. *Nature Communications*, 7, 10581. doi:10.1038/ncomms10581

Griffin, D. A., Middleton, J. H., & Bode, L. (1987). The tidal and longer-period circulation of Capricornia, souther Great Barrier Reef. *Australian Journal for Marine and Freshwater Research, 38*, 461–474.

Jakobsen, H. H., & Markager, S. (2016), Carbon-to-chlorophyll ratio for phytoplankton in temperate coastal waters: Seasonal patterns and relationship to nutrients. *Limnology and Oceanography, 61*, 1853-1868. doi:10.1002/lno.10338

Ji, R., Davis, C., Chen C., & Beardsley, R. (2008) Influence of local and external processes on the annual nitrogen cycle and primary productivity on Georges Bank: A 3-D biological–physical modeling study, Journal of Marine Systems, 73(1), 31–47. doi:10.1016/j.jmarsys.2007.08.002

Kämpf, J., & Chapman, P. (2016), Upwelling Systems of the World: A Scientific Journey to the Most Productive Marine Ecosystems. Springer International Publishing, Cham, 433 pp.

Kämpf, J., & Kavi, A., (2019) SST variability in the eastern intertropical Indian Ocean – On the search for trigger mechanisms of IOD events. Deep Sea Research Part II: Topical Studies in Oceanography, 166, 64–74. doi:10.1016/j.dsr2.2018.11.010

Luyten, P. J., Jones, J. E., Proctor, R., Tabor, A., Tett, P., & Wild-Allen, K. (1999), COHERENS—A coupled hydrodynamic-ecological model for regional and shelf seas: User documentation, MUMM Report, Manage. Unit of the Math. Models of the North Sea, Brussels, Belgium, 914pp.

Mann, K. H., & Lazier, J. R. N. (1991), Dynamics of Marine Ecosystems: Biological-Physical Interactions in the Ocean. Boston; Blackwell: 466 pp.

Mellor, G. L., & Yamada, T. (1982), Development of a turbulence closure model for geophysical fluid problems. *Reviews of Geophysics and Space Physics, 20,* 851–875.

Messié, M., Petrenko, A., Doglioli, A. M., Aldebert, C., Martinez, E., Koenig, G., et al. (2020), The delayed island mass effect: How islands can remotely trigger blooms in the oligotrophic ocean. *Geophysical Research Letters, 47*, e2019GL085282. https://doi.org/10.1029/2019GL085282

Munk, W. H., & Sargent, M.C. (1954), Adjustment of bikini atoll to ocean waves. *U.S. Geological Survey Professional Paper, 260 C*, 275-280.

Rogers, J. (2015), Field observations of wave-driven circulation over spur and groove formations on a coral reef. *Journal of Geophysical Research: Oceans, 118 (6)*, 3059–3073. doi:10.1002/2014JC010464

Shchepetkin, A. F., & McWilliams, J. C. (2005), The regional oceanic modeling system (ROMS): a split-explicit, free-surface, topography-following-coordinate oceanic model. *Ocean Modelling, 9 (4)*, 347–404. doi:10.1016/j.ocemod.2004.08.002

Smagorinsky, J. (1963), General circulation experiments with the primitive equation. 1: the basic experiment. *Monthly Weather Review, 91*, 99–164. Doi:10.1175/1520-0493(1963)091<0099:GCEWTP>2.3.CO;2

Spall, M. A., & Pedlosky, J. (2013) Interaction of Ekman layers and islands. *Journal of Physical Oceanography 43, 5,* 1028–41.

Sprintall, J., & Tomczak, M. (1992), Evidence of the barrier layer in the surface layer of the tropics, *Journal of Geophysical Research, 97(C5),* 7305–7316, doi:10.1029/92JC00407

Stoddart, R. (1965), The shape of atolls, *Marine Geology, 3(5),* 369–383. doi:10.1016/0025-3227(65)90025-3.

Watson, S. J., Whittaker, J. M., Lucieer, V., Coffin, M. F., & Lamarche, G. (2017) Erosional and depositional processes on the submarine flanks of Ontong Java and Nukumanu atolls, western equatorial Pacific Ocean*, Marine Geology, 392*, 122–139. doi:10.1016/j.margeo.2017.08.006

Watts, A. (2019), Science, seamounts and society. Geoscientist, 290(7), 10–16. doi:10.1144/geosci2019-039

Wu, Q., Yu, G., Ma, Z., Ma, S., & Wu, S. (2016), Preliminary study on the fisheries catches in South China Sea via light falling-net fishing method, *International Journal of Innovative Studies in Aquatic Biology and Fisheries (IJISABF), 2(5),* 1–4, doi:10.20431/2454-7670.0205001